Microb Ecol (1988) 16:253–270

MICROBIAL ECOLOGY

The Cryptoendolithic Microbial Environment in the Ross Desert of Antarctica: Mathematical Models of the Thermal Regime

James A. Nienow,[1] Christopher P. McKay,[2] and E. Imre Friedmann,[1]

[1]Polar Desert Research Center and Department of Biological Science, Florida State University, Tallahassee, Florida 32306-2043, USA; and [2]Solar System Exploration Branch, NASA Ames Research Center, Moffett Field, California 94035, USA

Abstract. Microbial activity in the Antarctic cryptoendolithic habitat is regulated primarily by temperature. Previous field studies have provided some information on the thermal regime in this habitat, but this type of information is limited by the remoteness of the site and the harsh climatic conditions. Therefore, a mathematical model of the endolithic thermal regime was constructed to augment the field data. This model enabled the parameters affecting the horizontal and altitudinal distribution of the community to be examined. The model predicts that colonization should be possible on surfaces with zenith angle less than 15°. At greater zenith angles, colonization should be restricted to surfaces with azimuth angles less than 135° or greater than 225°. The upper elevational limit of the community should be less than 2,500 m. The thermal regime probably does not influence the zonation of the community within a rock.

Introduction

The climate in the elevated regions of the Ross Desert (unofficial name for the ice-free region of southern Victoria Land, Antarctica; the region is also known as the "dry valleys") is characterized by low temperatures and little precipitation. Under these conditions, life is restricted to only a few habitats. Chief among these is the pore space within translucent sandstones, where a relatively rich community of microorganisms exists [5, 7, 8, 9, 20]. However, not all porous rocks in the region are colonized, and in some cases, only surfaces oriented toward the north are colonized whereas south-facing surfaces of the same rock are apparently abiotic. This distribution suggests that, although the environmental conditions in the cryptoendolithic habitat are more favorable to life than are the external conditions, there is still a limit on colonization imposed by the external environment and that this limit is connected with the physical properties and geographic location of the rock and the orientation of its surfaces. In this paper, we examine the factors contributing to the thermal regime in the cryptoendolithic habitat and then use the information to predict the range of the cryptoendolithic community.

The biological significance of the thermal environment at the air-rock interface was first investigated by Jaag [14]. Since then, numerous studies of the temperature regime in the lithic and edaphic environments have been published. Works of general interest have been reviewed by Friedmann and Galun [6] and Kershaw [18]; studies in the Ross Desert include those of Friedmann et al. [5, 11, 16, 17, 20] and Miotke [21]. The approach usually taken in these studies is the direct field measurement of the thermal regime. This approach requires either human presence or the use of automatic recording devices and is therefore limited in the number of sites that can be measured. Here we use a complementary approach: the construction of mathematical models, which predict the thermal regime in the lithic environment from standard meteorological data. This approach allows the estimation of the thermal regime under a wider range of conditions than can be measured practically. In addition, hypotheses concerning the causes of observed temperature patterns can also be tested through model experiments in which single parameters vary; such experiments cannot be carried out under field conditions.

Materials and Methods

Description of the Model

The temperature profile in a colonized rock is calculated by solving the one-dimensional equations of heat transfer for a finite solid. The absorption of shortwave radiation within the rock is included in the formulation so that the effect of the translucence of colonized rocks on the temperature profile can be investigated.

The system of equations considered in the model is given by

$$\rho c \frac{\partial T}{\partial t} = \frac{\partial}{\partial z}\left(S - k \frac{\partial T}{\partial z}\right) \tag{1}$$

subject to the boundary conditions

$$\begin{aligned} Q &= S + L_s - L_r - C - k\frac{\partial T}{\partial z} && z = 0, \quad t > 0 \\ Q &= 0 && z = D, \quad t > 0 \\ T(z) &= T_{init}(z) && t = 0, \quad 0 \le z \le Z_t \end{aligned} \tag{2}$$

where T(z) is the temperature at depth z and time t. The left-hand side of equation (1), where ρ is the density and c the heat capacity of the rock, represents the rate of energy storage in the layer. Q is the total energy flux across the plane parallel to the surface at depth z; Q is divided into the flux of shortwave solar radiation (S), the flux of longwave radiation from the sky (L_s), the flux of longwave radiation leaving the rock (L_r), the convective energy flux to the air (C), and the conductive energy flux, $k\frac{\partial T}{\partial z}$. Evaporation is not considered in the present paper; evaporation and the moisture regime in general will be considered in a future paper. Note, however, that the potential evaporation in the region is only 1–2 mm day^{-1}, equivalent to an average heat flux of 30–60 Watts m^{-2}, and the actual evaporation rate is significantly lower.

The individual terms of equations (1) and (2) are considered in detail in the sections that follow.

Shortwave Solar Radiation (S)

Incident Flux. The incident shortwave (300–2,500 nm) radiation is the sum of the direct solar radiation (S_d), the diffuse shortwave sky radiation (S_f), and the diffuse radiation reflected from the surrounding terrain (S_r) striking its surface. These terms are calculated according to the following set of equations.

1. The direct radiation (S_d) striking a sloped surface is the product of the direct radiation striking a surface perpendicular to the sun's rays (S_{max}) and the cosine of the angle ϕ between the normal to the surface and the angle of the sun's rays, i.e.,

$$S_d = S_{max}\cos(\phi). \tag{3}$$

S_{max} and ϕ are functions of the latitude of the site, the declination of the sun, and the time of day; ϕ is also a function of the zenith angle, ζ_r, and azimuth angle of the surface [12]. The declination of the sun is approximated by its noontime value:

$$\delta = 23.45°\cos(360°D/365) \tag{4}$$

where D is the number of days since June 22 and 23.45° is the maximum solar declination. The latitude of the site, the day of the year, and orientation of the surface are determined by the situation modeled.

S_{max} is calculated from

$$S_{max} = S_c\tau^{-m} \tag{5}$$

where S_c is the solar constant (1,360 watts m^{-2}), τ is the transmissivity of the atmosphere, and m is the relative distance traveled by the sun's rays through the atmosphere—m = 1.0 if the solar zenith angle, ζ_s, is 0.0. For zenith angles less than 80°, m is approximated by $\sec(\zeta_s)$. For zenith angles between 80 and 90°, the approximation

$$m = [\cos(\zeta_s) + 0.025\exp(-11\cos(\zeta_s))]^{-1} \tag{6}$$

is used [19]. For larger zenith angles, the sun is below the horizon, and S_{max} is set equal to 0.0.

2. The diffuse radiation striking a surface is, in general, a function of the water and aerosol content of the atmosphere, the reflectivity of the underlying terrain, and the zenith angle of the sun [25]. Lacking a precise formulation of S_f, the approximation

$$S_f = fS_{max} \tag{7}$$

is used. The coefficient f is a constant.

For sloped surfaces, S_f is multiplied by a correction factor, v_s, which takes into account the fact that the hemisphere above the surface includes the surrounding terrain as well as sky. v_s is given by Robinson [25] as

$$v_s = \cos^2(\zeta_r/2) \tag{8}$$

3. The reflected radiation striking a surface is calculated as the product of the light reflected from a horizontal surface and a factor determined by the slope of the surface:

$$S_r = r_g[S_{max}\cos(\zeta_s) + fS_{max}]v_g \tag{9}$$

r_g is the reflectivity of the surrounding terrain. v_g is given by Robinson [25] as

$$v_g = \sin^2(\zeta_r/2) \tag{10}$$

Internal Flux. The distribution of shortwave radiation within the upper 5 cm of the rock is approximated by

$$F^- = (S_d + S_f + S_r)\exp(-pz) \tag{11}$$

$$F^+ = rF^-{}_0\exp(-pz) \tag{12}$$

where F^- represents the flux directed into the rock, F^+ represents the flux directed out the rock, p

is the bulk extinction coefficient, and r is the shortwave reflectivity. Because the typical values of p are large (see below), F^- and F^+ are assumed to be zero below 5 cm. The total flux has been divided into upward and downward components to emphasize that the radiation regime is not strictly determined by absorption but also includes scattering effects.

Absorbed Longwave Sky Radiation (L_s)

Unlike shortwave radiation, longwave thermal radiation from the sky is assumed to be absorbed in the surface layer of the rock. This assumption is based on the high absorptivity of quartz in the thermal wavelengths. The equation used is

$$L_s = e_g(1.195\sigma T_a^4 - 170.9)v_s \tag{13}$$

where e_g is the emissivity of the surface, σ is the Stefan-Boltzmann constant, and T_a is the air temperature (°K). This equation makes use of the empirical formula for thermal sky radiation derived by Swinbank [28] from measurements in Australia.

Emitted Longwave Radiation (L_r)

The emission of longwave radiation from the surface of the rock is given by

$$L_r = e_g(\sigma T_0^4)v_s \tag{14}$$

where T_0 is the surface temperature and e_g is the emissivity of the rock.

Convection

The convective flux of thermal energy is approximated by

$$C = h(T_0 - T_a) \tag{15}$$

where h is a proportionality coefficient dependent on the wind speed and the geometry of the surface. The dependence of h on wind speed and surface geometry is complicated [12, 22]. These relationships are simplified by assuming that convection coefficients calculated for horizontal surfaces provide a reasonable approximation of the coefficients for sloped surfaces. The error in this assumption is greatest for vertical surfaces during periods of very low wind speeds. At such times the absolute magnitude of the convective loss is low, and therefore the overall effect of the error on the temperature gradient within the rock should also be low. Convection is divided into three domains based on the relative sizes of the Grashof number (N_{Gr}) and the Reynolds number (N_{Re}). The Nusselt number (N_{Nu}), given by

$$N_{Nu} = h\Delta/k_a \tag{16}$$

where k_a is the thermal conductivity of the air and Δ is the characteristic dimension of the rock, is then estimated from the corresponding equations [22].

Domain 1. $N_{Gr} > 16N_{Re}^2$. In this domain free convection dominates and N_{Nu} can be approximated by

$$N_{Nu} = 0.530(N_{Gr}N_{Pr})^{0.25} \tag{17}$$

where N_{Pr} is the Prandtl number.

Domain 2. $N_{Gr} < 0.1N_{Re}^2$. Here forced convection dominates. Under the additional assumption of turbulent flow N_{Nu} is given by

$$N_{Nu} = 0.032N_{Re}^{0.8} \tag{18}$$

Domain 3. $0.1N_{Re}^2 < N_{Gr} < 16N_{Re}^2$. This is a transition zone between free and forced convection. N_{Nu} is calculated according to both methods, and the larger value used.

Method of Solution

The temperatures are calculated by means of a Crank-Nicolson mid-difference scheme [3] and a grid with varying mesh size. The thermal properties of the rock are assumed to be uniform within each layer defined by the mesh points but can vary from layer to layer. The total depth of the grid is treated as an input parameter.

The solution method requires that all terms in equation (1) that are functions of temperature be treated as linear functions of temperature. Both L_s and L_r contain quartic factors in T. These are linearized at each time step by the substitution of $(T_{old})^3T$ for T^4, where T_{old} is the temperature computed at the previous time step.

The solution algorithm was checked against analytical solutions for simple problems [2]. For the problems tested, the agreement between the two solutions was better than 0.01°C.

Environmental Parameters

Time. For the purposes of this paper, the day was fixed as December 22 (D = 182), the Antarctic summer solstice, when the solar radiation is at its maximum. The bulk of the detailed microclimate measurements at the principal cryptoendolithic study site, Linnaeus Terrace, were taken around this time, so comparisons between field data and model results are possible.

Macroclimate. The macroclimate factors used in the model include the air temperature and wind speed above the boundary layer and the solar radiation regime. Generally, air temperature and wind speed are held constant at −12.5°C and 2.7 m s^{-1}, respectively. These were the mean values on Linnaeus Terrace during the month of December 1981 (data supplied by the Automatic Weather Station group based at the University of Wisconsin [26, 27]).

The equations used to calculate the radiation regime contain three parameters, which were treated as independent of time and surface orientation. The transmissivity of the atmosphere (τ) was set at 0.80 in keeping with the clarity of the air over Antarctica [12]. A value of 0.13 was then chosen for the ratio of S_f to S_{max}. This combination of τ and f provides a good fit for measured values of visible light striking a horizontal surface on Linnaeus Terrace, especially when the sun is high above the horizon (see ref. 11). The reflectivity of the surrounding terrain (r_g) was set at 0.25—near the low end of measured reflectivities (see below).

Rock Parameters

Geometric Parameters. The orientation of the surface was dependent on the application of the model under consideration. The basic effects of surface orientation on the temperature regime are discussed in detail below.

The characteristic dimension (Δ), a measure of the horizontal dimensions of a rock or stone, was set at 50.0 cm. Although this choice is somewhat arbitrary, it is similar to the observed dimensions of colonized surfaces.

The total depth of the temperature profile was set at 11 m. This choice of Z_t eliminates artifacts caused by the assumption of no flow of energy across the lower boundary for model periods of 1–10 days. The amplitude of the diurnal temperature wave is reduced to 1% of its surface value at about 1 m.

The grid used in calculating the temperature profile was varied according to the time step of the application. For models of the diurnal temperature regime, the mesh distance was set at 1.0 cm

for the first 10 cm, 2.0 cm for the next meter, and 50.0 cm for the final 10 m. For models of shorter time intervals, the mesh was reduced to 0.1 cm for the first 5 cm. The same grids were used for outcrops and thin stone plates.

Thermal Properties. Because of expected variability between sites, the mass density, heat capacity, and thermal conductivity of colonized rocks from Linnaeus Terrace were measured directly. The mass density and porosity were determined by comparing the weights of samples dry and saturated with carbon tetrachloride [23]. The heat capacity was measured using 400 ml Dewar flasks as calorimeters.

Thermal conductivity was measured by a custom technique. Type T thermocouples were attached to both sides of disks of rock approximately 3.0 cm in diameter and 0.5 cm thick. The lower surface of the disk was placed on a layer of medium-grained quartz sand maintained at about 90°C by a temperature-controlled hot plate. A disk of silicon rubber (RTV 11, Dow Corning) of similar dimensions and with a similar thermocouple arrangement was placed on top of the rock disk. Both disks were surrounded by rings of silicon rubber, and the system was allowed to equilibrate for 2–3 hours.

After equilibration, assuming the same heat flux across the two disks, the rock conductivity can be calculated from

$$k_s A_s(\Delta T_s/\Delta X_s) = k_r A_r(\Delta T_r/\Delta X_r)$$

where k is the thermal conductivity, A is the area of the disk, ΔT is the temperature drop across the disk, ΔX is the thickness of the disk, and s and r refer to silicon rubber and rock, respectively [2]. A value of 0.0030 W cm^{-1} $°C^{-1}$ (Dow Product Sheet) was used for k_s.

Measured values for the density, porosity, and heat capacity are given in Table 1. Thermal conductivities are given in Table 2. All values are in the range reported for sandstones [2]. For outcrops, the respective means of the measured values were used for the entire profile. For models of thin stone plates resting on soil, the measured values were used only for the rock and not for the underlying soil. Layers in the soil were assigned a mass density of 1.95 g cm^{-3}, a heat capacity of 0.80 joules g^{-1} $°C^{-1}$, and a thermal conductivity of 0.0025 W cm^{-1} $°C^{-1}$. These values were not measured. The mass density and heat capacity were estimated under the assumption that the soil had a porosity of 75% and that the chief source of its components was weathered sandstones. The thermal conductivity was then chosen to give a thermal diffusivity in agreement with the measured value of 0.0016 cm^2 s^{-1} [24].

Radiative Properties. Reflectivity was measured by means of an adaptation of the method of Graser and Van Bavel [13]. A light pipe was attached to a light sensor (Licor 185, Lambda Instruments) that measures light in the photosynthetically active region spectrum (PAR, 400–700 nm). The field of view of the light pipe was restricted by a black cylinder. The end of the light pipe was held 2.0 cm above the surfaces of large plates of colonized Beacon sandstones illuminated by sunlight. The measured light values were compared with the light reflected from a 1-cm-thick layer of powder magnesium carbonate ($r = 0.95$) and from a grey cardboard (Kodak, $r = 0.19$).

The measured reflectivities on a single colonized rock surface ranged from 17 to 42%. Although the distribution of the cryptoendolithic community and its relation to the reflectivity of the surface have not been investigated in detail, organisms seem to be associated with regions of light to medium staining (reflectivity 23–30%). In the model, the reflectivity is set at 30%. It is also assumed that the reflectivity in the near infrared (700–2,500 nm) does not vary significantly from the reflectivity in the PAR. This assumption is justified in part by the relatively flat absorption spectrum of quartz in this region.

The downward flux of light was measured by the insertion of the light pipe-light sensor combination into holes drilled from the bottom of a rock to within 1 cm of the surface. The light levels obtained were compared with the light level measured with the rock removed. The thickness of the crust above the light pipe was measured with a machinist's micrometer. After a measurement, the hole was drilled further and the light transmission and rock thickness were remeasured. This process was continued as long as possible. The extinction coefficient of the rock was determined by means of equation (12).

Table 1. Density, porosity, and heat capacity of colonized rocks from Linnaeus Terrace

Sample	Dry weight (g)	Density (g cm^{-3})	Porosity (%)	Heat capacity (J g^{-1} $°C^{-1}$)
1 O-B[a] Medium[b]	16.15	2.31	11.1	0.73
2 O-B Medium	44.88	2.40	6.1	0.83
3 O-B Medium	35.58	2.34	8.3	0.80
5 Silicified	44.06	2.32	8.7	0.79
6 R-O Medium	18.83	2.31	10.5	0.82
7 B Medium	21.71	2.26	13.0	0.73
8 B Medium	43.91	2.34	8.9	0.78
9 B Medium	23.21	2.33	12.3	0.93
10 W Fine	38.57	2.53	2.3	0.84

[a] O = Orange, B = Brown, R = Red, W = White
[b] Medium and fine refer to the average grain size of the sample, i.e., between 0.3 and 0.5 mm in medium-grained samples and 0.1 and 0.2 in fine-grained samples

Table 2. Thermal conductivity of colonized rocks

Sample	Thickness (cm)	Conductivity (W cm^{-1} $°C^{-1}$)
Surface crust	0.45	0.020[a]
Surface crust	0.57	0.025[a]
Red bedrock	0.50	0.024
White fine-grained sandstone	0.37	0.030
Light bedrock	0.40	0.023

[a] Average of two measurements

Extinction coefficients for five samples ranged from 12 to 29 cm^{-1}, depending on the degree of silicification, the presence of iron oxides and organisms, and the grain size. In general, the extinction coefficient was set at 19 cm^{-1}.

The long-wave emissivity of the surface (eg) was set at 0.95. This value was not measured but is in keeping with the high quartz content of the colonized materials.

Initial Temperature Profiles. During early investigations of the model, the system was assumed to be isothermal at the beginning of the model period. This assumption leads to obvious errors in the diurnal temperature regime similar to those reported by Buchan [1]. In the present study, artificial initial temperature profiles were constructed as follows. The temperature regime for each orientation and set of thermal properties was calculated for the time period $171 \leq D \leq 181$, with a large time step and the assumption of an isothermal initial profile. The final temperature profiles from these calculations were then used as the initial profiles for $D = 182$.

Results and Discussion

The utility of the model is best demonstrated through the application of the model to the Antarctic cryptoendolithic ecosystem. Two aspects of the eco-

system were chosen for investigation with the model: the relationship of internal temperature gradients to the external environment and the relationship between the orientation and position of a surface and the probability of colonization by the endolithic community.

The Control of Internal Temperature Gradients

In this section, the roles of internal light gradients and fluctuations in the wind in the production of temperature gradients in the upper 4.0 cm of colonized sandstones are examined by applying the model. This study was prompted by the finding of temperature maxima 1 cm below the surface of colonized rocks and rapid temperature fluctuations about 0°C at the surface [20]. Accordingly, for the model the orientation of the surface was fixed at azimuth 45°, zenith 66° to approximate the orientation of the "warm" surface described by McKay and Friedmann [20].

The effects of light and wind were studied separately. In the light studies the wind was held constant at 2.7 m s^{-1}. Three extinction coefficients spanning the measured range were used. The case of all light absorbed in the surface layer was also modeled for comparative purposes. In the wind studies, the wind was held constant at 2.7 m s^{-1} until 10:00; at 10:00 the average speed was doubled. A sinusoidal fluctuation with an amplitude of 2.7 m s^{-1} and a period of either 3 or 10 min was superimposed on the doubled speed. The periods of the fluctuations were chosen to represent the range found by McKay and Friedmann [20]. The speeds used are arbitrary and chosen for the purpose of illustration alone. During the period of fluctuating winds, the time step of the solution algorithm was reduced to 1 sec.

The effects of changing the extinction coefficient are illustrated in Fig. 1. There are two points of interest in this figure. First, the temperature of the colonized slab increases and decreases as a unit. The temperature gradient does not exceed 2.5°C over the 4.0 cm at any time. This implies that diurnal temperature variations are not an important parameter leading to the observed stratification in the community, in agreement with the observations of McKay and Friedmann [20].

Second, during periods of warming, the surface is within 0.1°C of the temperature at 0.4 mm for all of the extinction coefficients examined (spanning the range measured in the laboratory). This finding is contrary to those of Kappen et al. [17] and McKay and Friedmann, who reported temperature differences of as much as 2°C. This discrepancy is caused in part by the use of constant winds in the model, a situation that rarely holds in the field. If winds are allowed to vary, then surface temperatures lower than the temperatures of the layers immediately below can occur, as illustrated by the results of the wind experiments shown in Fig. 2. The translucence of the rocks, however, plays only a secondary role in this phenomenon.

To match the profiles reported in McKay and Friedmann completely, not even the inclusion of variable winds is sufficient. This result may indicate the presence of a strong depth dependence in the thermal conductivity function in the upper 5 mm of colonized rocks, perhaps caused by the activity of the

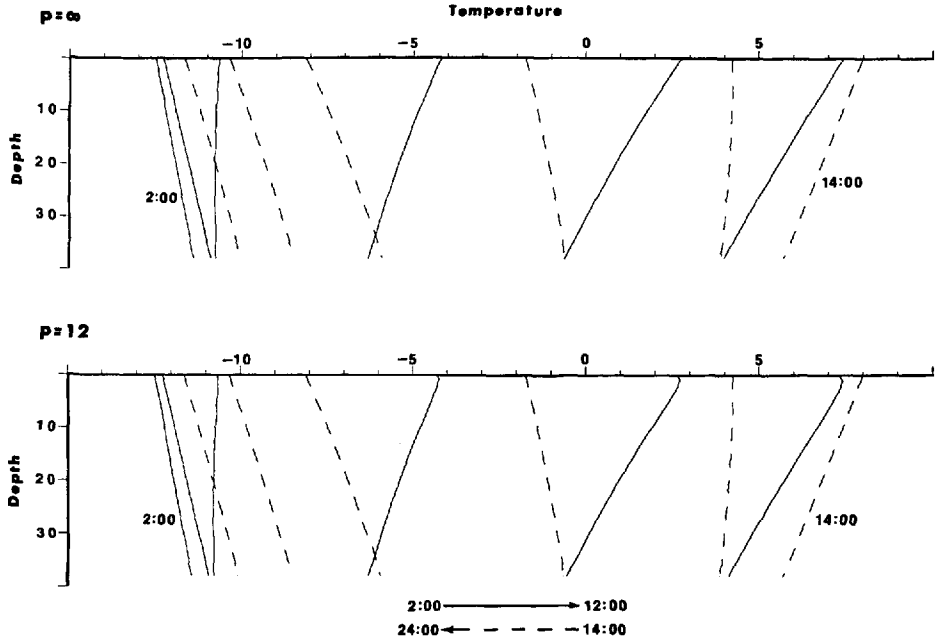

Fig. 1. Computer simulations of effects of the penetration of light on internal temperature profiles, December 22. The depth is given in millimeters, the temperature in °C, time in hours with 12:00 equal to solar noon. Solid lines represent temperature profiles at even hours between 2:00 and 12:00, counted from the left. Dotted lines represent temperature profiles at even hours between 14:00 and 24:00, counted from the right. Two extinction coefficients are shown, $p = \infty$ and $p = 12$. Over the range of extinction coefficient tested, light penetration has little effect on the internal temperature regime.

organisms. It is possible, however, that the surface sensors in the field are biased toward the air temperature because of a poor thermal contact with the surface.

The results shown in Fig. 2 are consistent with another finding of McKay and Friedmann. If the amplitudes of the temperature wave at the surface and at 0.4 are compared for winds of 3 or 10 min periods, the ratios of the amplitudes are 0.6 and 0.8, respectively. Although these are higher than the ratios of 0.54 and 0.56 reported from the field for two occasions of fluctuating winds, they indicate that the observed temperature oscillations are indeed caused by short-period wind fluctuations. The difference in the values is a further indicator of either a depth dependence in thermal conductivity or a poor thermal contact affecting the field measurements.

Range of Cryptoendolithic Community

Effect of Surface Orientation. Field observations indicate that the colonization of a sandstone surface in Antarctica is strongly correlated with the orientation of the surface and that the causal factor of the correlation is probably the

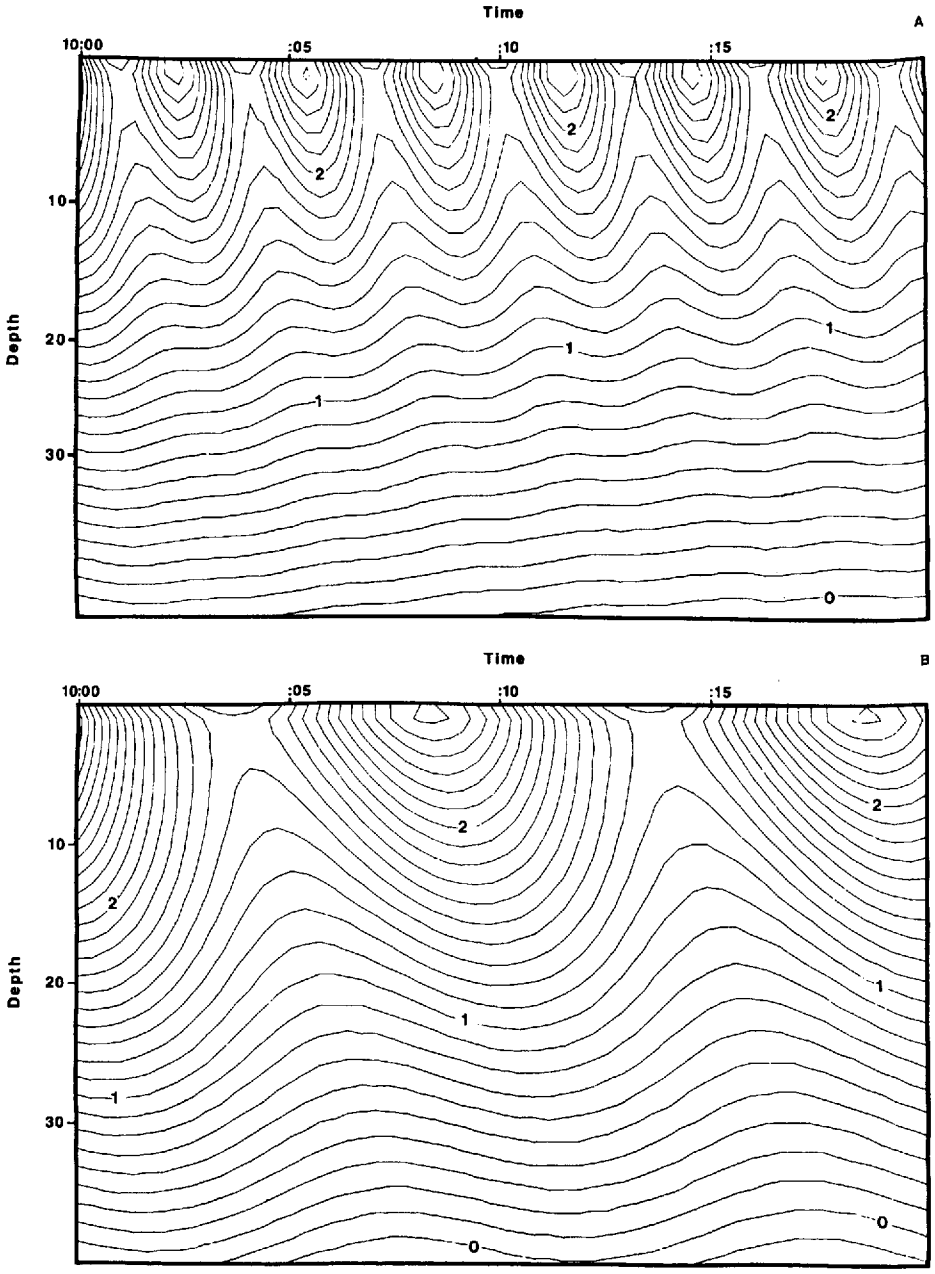

Fig. 2. Computer simulations of effects of varying wind speeds on internal temperature profiles, December 22. The depth is given in millimeters. Temperature contours are drawn at intervals of 0.1°C. In both figures, the average wind speed is 5.4 m s^{-1} and the amplitude is 2.7 m s^{-1}. In (**A**) the period of the fluctuation is 3 min; in (**B**) the period is 10 min. The amplitude of an internal temperature wave caused by a short-term fluctuation in wind speed can be on the order of 1°C. However, the effect on the direction of the internal temperature gradient is slight.

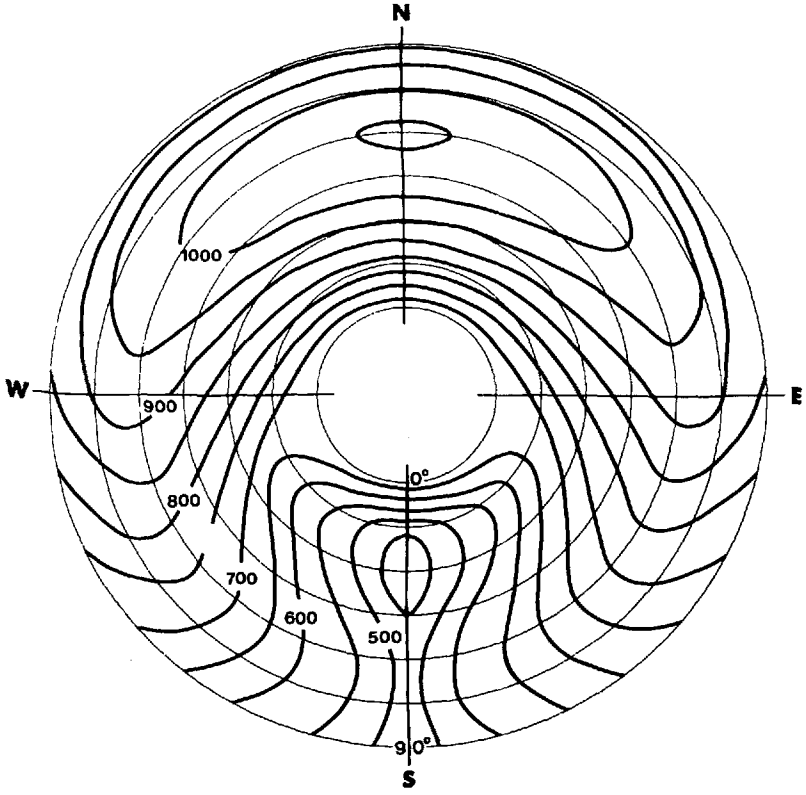

Fig. 3. Computer simulations of dependence of maximum incident light intensity on surface orientation, December 22. Contours are drawn at intervals of 50 W m^{-2}. The 0° zenith angle has been expanded to emphasize the importance of this orientation in the field.

temperature regime of the surface [4, 5, 17, 20]. In this section the relationship between surface orientation and the diurnal temperature and shortwave radiation regimes is investigated. Two basic models of colonized material—outcrops of bedrock and thin, sandstone plates resting on thick soil—are used. For outcrops, the zenith angle was varied from 0 to 90° in 15° intervals, and the azimuth angle was varied from 0 to 315° in 45° intervals for a total of 49 orientations. For boulders and thin stone plates, fewer orientations were used because the general patterns are similar to those of outcrops.

The relationship between surface orientation and incident radiation can be seen in Figs. 3 and 4. All surfaces are exposed to considerable radiative energy fluxes at some time of the day. The radiation maxima range from 400 W m^{-2} for moderately sloped, south-facing surfaces to 1,060 W m^{-2} for moderately sloped, north-facing surfaces; the maximum flux incident on a horizontal surface is 660 W m^{-2}.

The shape of the radiation curves is also of interest because of the effect it has on the shape of the temperature curves. With the exception of the horizontal surface, the diurnal course of the incident radiation (Fig. 4) is markedly non-

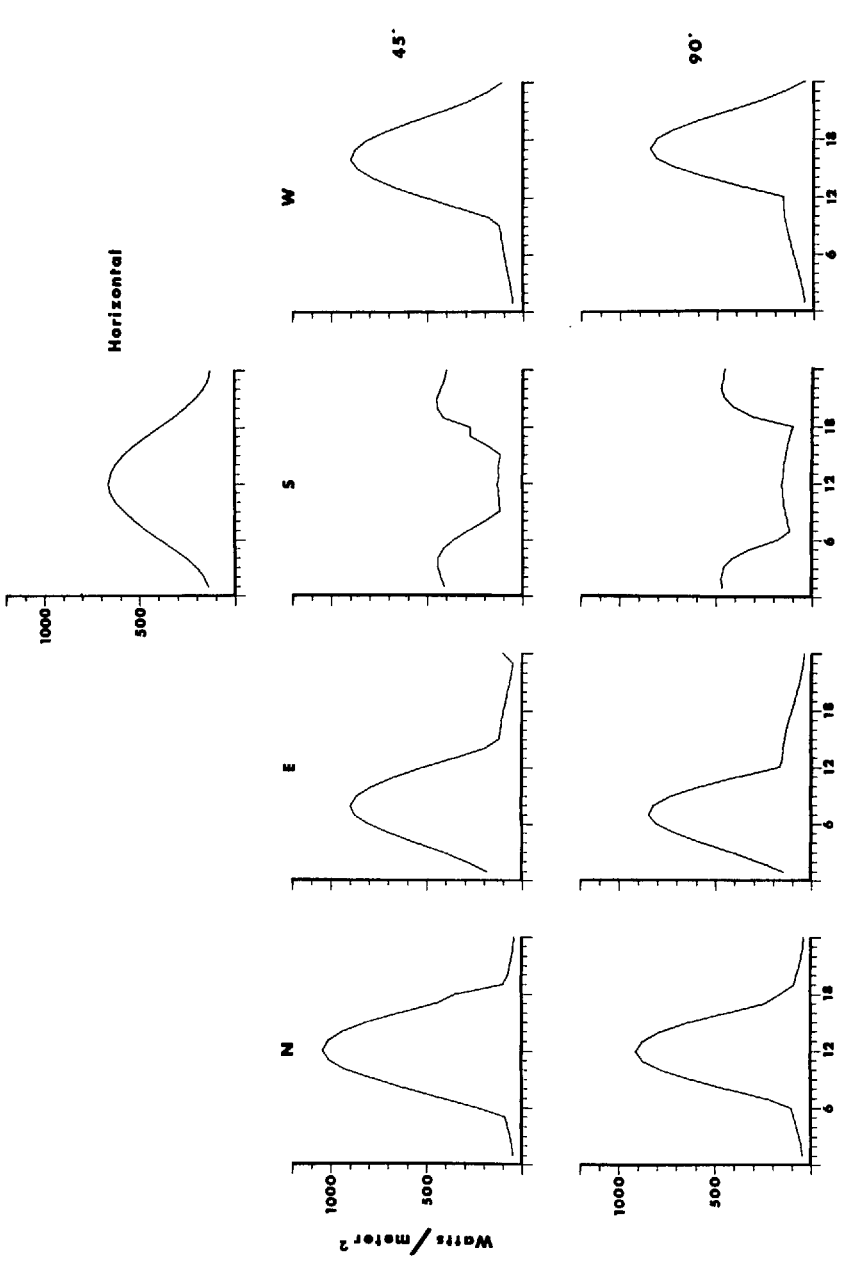

Fig. 4. Computer simulations of diurnal variation of incident radiation at selected orientations, December 22. Note the asymmetry between east- and west-facing surfaces and the double peak in south-facing surfaces.

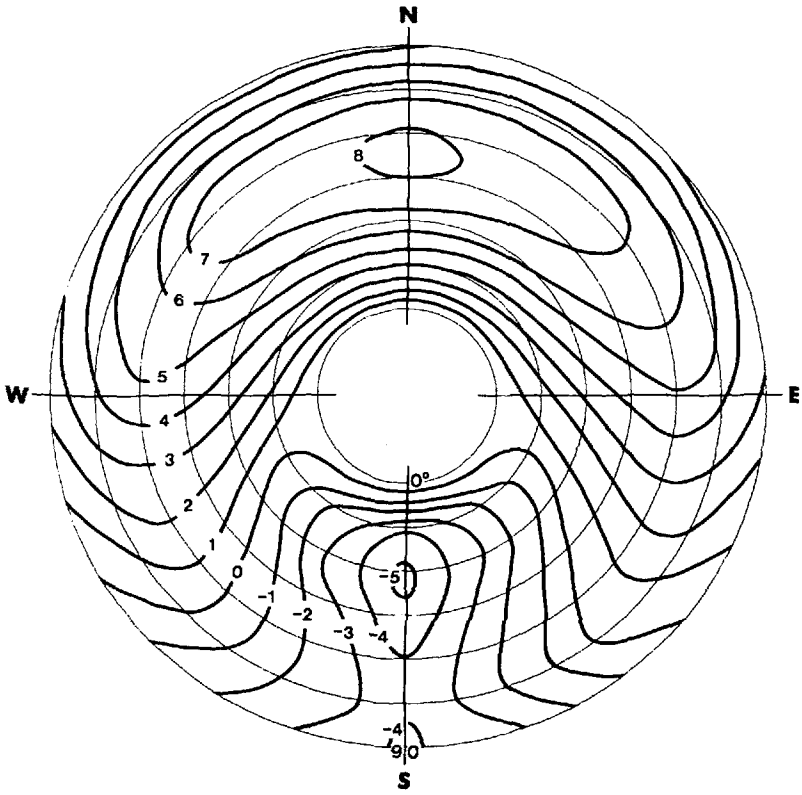

Fig. 5. Computer simulations of dependence of maximum surface temperature on surface orientation, December 22. Contours are drawn at intervals of 1°C. The 0° zenith angle has been expanded to emphasize the importance of this orientation in the field. There is a slight asymmetry between east- and west-facing surfaces.

sinusoidal; each sloped surface spends some part of the day in the shadow. At azimuths away from 0 and 180°, the curves are asymmetric as well. For east-facing surfaces, the elevation of the sun above the horizon, and therefore the level of irradiation, is greater after the time of maximum irradiation than before. The opposite is true for west-facing surfaces. South-facing surfaces have paired maxima occurring at about 02:00 and 22:00 even though the sun remains above the horizon; the low solar elevation at midnight results in increased absorption of direct solar radiation by the atmosphere.

The dependence of the daily surface temperature regime on orientation of rock outcrops can be seen in Figs. 5 and 6. The general patterns are similar to those seen in the radiation isopleths. The temperature maxima range from about −5.5°C for south-facing surfaces to about +8.2°C for moderately sloped north-facing surfaces; horizontal surfaces have a maximum of +0.7°C. These figures translate into an approximate increase in the maximum surface temperature of 1.0°C for every 50 Watts m^{-2} increase in maximum irradiation. Temperature minima are within 2.5°C of air temperature (−12.5°C) for all

orientations; horizontal surfaces have the highest minima and east-facing surfaces the lowest. The diurnal variation in temperature ranges from about 9°C for south-facing surfaces to about 21°C for moderately sloped north-facing surfaces; the diurnal variation for a horizontal surface is about 11°C. All of these results fit well with previous field data [4, 17, 20]. The differences can easily be attributed to the use of constant wind and air temperature regimes in the present study and to the uncertainty of the reflectivity and orientation of the surfaces monitored in the field.

The curves (not shown) for colonized stone plates 5.0 cm thick resting on soil are similar to those for outcrops. The major difference is that, for a given orientation, the maximum temperature is about 1°C higher and the diurnal variation correspondingly greater. This difference is due to the less efficient transfer of energy to the lower layers.

An additional point of interest in these results is the timing of the temperature maximum with respect to the time of the maximal incident radiative flux. The temperature maximum is usually assumed to occur 3 hours after the radiation maximum. The temperature maxima in Fig. 6 occur between 1 and 2 hours after their corresponding radiation maxima. This discrepancy is due to the common, but in this case false, assumption that the diurnal radiation and temperature regimes are sinusoidal.

In order to examine the effects of the differing thermal regimes on colonization, the relative net photosynthesis, NP, was estimated from the empirical equation

$$NP = \{2[(T_{opt} - T_{min})^2(T - T_{min})^2] - (T - T_{min})^4\}/[(T_{opt} - T_{min})^4]$$

where T_{opt} is the optimal temperature for net photosynthesis and T_{min} is the minimum temperature [15]. Previous studies [16, 29] indicate that T_{opt} is about +8°C and T_{min} is about −10°C for the cryptoendolithic community. NP was integrated for the entire year and the results were normalized by the maximum value obtained. The results are shown in Fig. 7. Although some photosynthesis is possible for all orientations, there is an order-of-magnitude difference in the photosynthetic potential of difference surfaces. This difference can be used to explain some of the observed patterns of colonization. Because rates of photosynthesis are low even under optimal conditions [16], it is probable that, at a substantial fraction of the maximal yearly photosynthetic carbon uptake, the increase in biomass and cell numbers is not sufficient to offset losses. The value of this fraction must be less than 0.4, because horizontal surfaces are well colonized, but may well be as high as 0.3. If 0.3 is the cutoff point, then we would not expect to find colonization on the surfaces of outcrops facing southeast-south-southwest that have a zenith angle greater than 15°.

For other orientations there should be a correlation between the degree of colonization and the zenith angle of the surface. The effect should be strongest for surfaces facing northeast-north-northwest with zenith angles between 0° and 30°. At zenith angles above 30°, the dependence of temperature, and therefore net photosynthesis, on zenith angle is weaker. At these angles the correlation of colonization with angle may be obscured by other considerations, such as moisture.

The slightly warmer temperature regimes in stone plates mentioned earlier

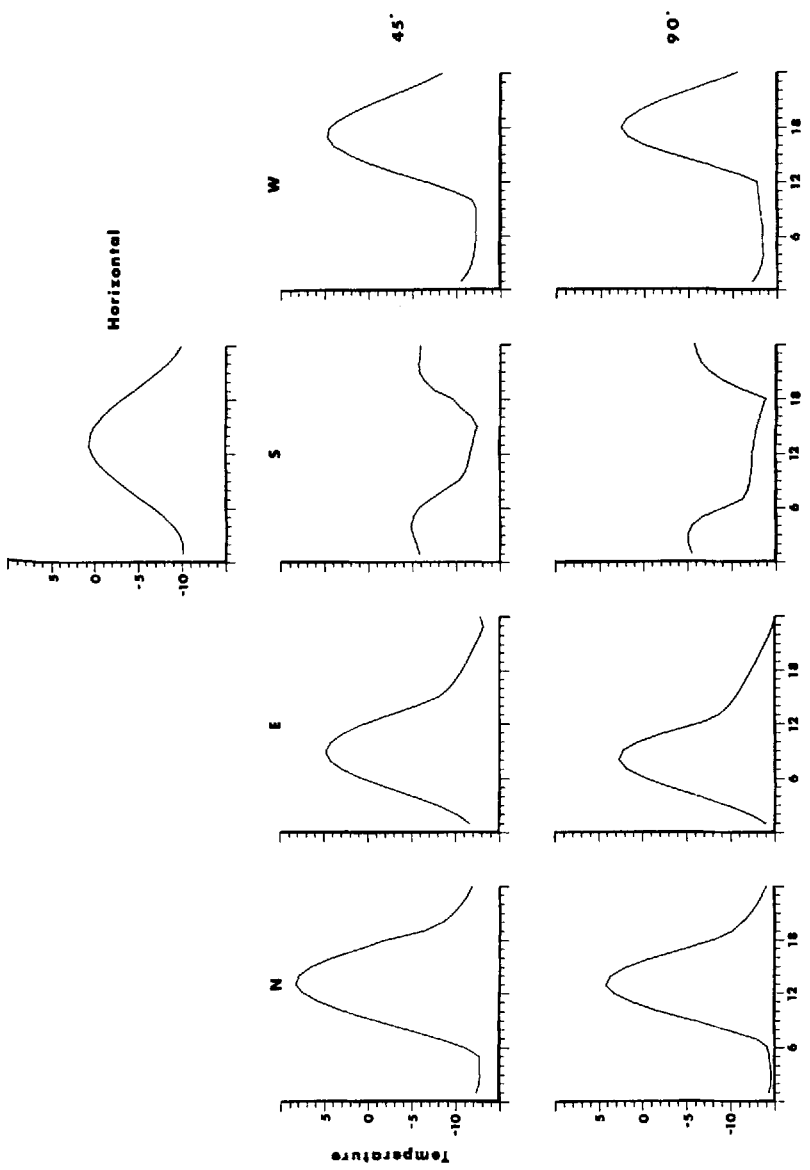

Fig. 6. Computer simulations of diurnal variation of surface temperature for selected orientations, December 22. The temperature curves follow the light curves (Fig. 4) closely, with only a slight delay between the time of maximum irradiation and the time of maximum temperature.

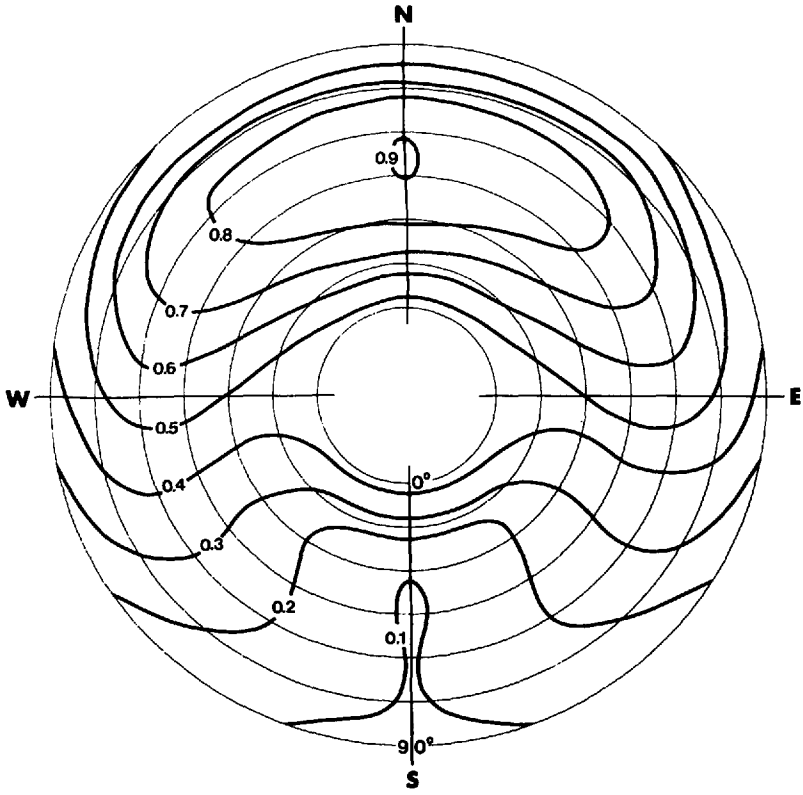

Fig. 7. Computer simulations of relative annual photosynthetic gain (NP) as a function of surface orientation. The 0° zenith angle has been expanded to emphasize the importance of this orientation in the field. Colonization is probably restricted to orientations with annual photosynthetic gains greater than about 30% of the expected maximum.

may extend the range of colonizable stone surfaces. In particular, if temperature is the only constraint then horizontal stones should sustain greater growth than horizontal outcrops.

The effects of surface orientation on microbial colonization are especially apparent in the field when colonized ledges fall or when small colonized stones are moved by wind. If such events are accompanied by a change of sufficient magnitude in the orientation of the surface, cell death and silicification of the rock surface occur [10]. After additional changes in orientation, the surface can be recolonized. Thus, smaller clasts that have been repeatedly turned over by the wind show traces of several distinct colonization events.

Effect of Altitude. As just discussed, the range of the cryptoendolithic community at any elevation is limited to rock surfaces with the proper orientation. This leaves the question of the elevational limits of the community. In particular, are the peaks of Antarctica's higher mountains capable of sustaining the cryptoendolithic community, and could they serve as refuges for the community during periods of glaciation?

In order to address these questions, the orientation of the surface was fixed at azimuth 0° and zenith 52.5°. This orientation yields the highest surface temperature (see Fig. 5). The mean air temperature was then varied from −25° to 0° in 5° intervals.

Over the range studied, difference between the maximum surface temperature and the air temperature is nearly constant, varying between 20.1 and 21.6°C. This result is not unexpected because the major point of entry for air temperature is in the convection equation (15), which is linear in T_a. Of more interest are the implications this result has for the expected elevational distribution of the cryptoendolithic community. If it is assumed that this result holds for other orientations (a reasonable assumption in light of equation (15)) and that the adiabatic lapse rate for air temperature is −9°C for every 1,000 m of elevation then, using Figs. 5 and 7 for reference, at an elevation of 2,100 m (500 m higher than Linnaeus Terrace) the cryptoendolithic community should be restricted to sloped, north-facing surfaces. It is probable that by 2,500 m, the community has disappeared completely, although field confirmation of this boundary is still necessary. Certainly, however, the peaks of the higher mountains, e.g., Mt. Lister which is over 4,000 m in elevation, are too cold to support the cryptoendolithic community and could not have served as refuges.

Acknowledgments. This research was supported by a Florida State University Fellowship to JAN and by National Science Foundation Grants DPP 80-17581 and DPP 83-14180 and National Aeronautics and Space Administration Grant NSG 7337 to EIF.

References

1. Buchan GD (1983) Predicting bare soil temperature. III. Extension to single-day variation. J Soil Science 33:365–373
2. Carslaw HS, Jaeger JC (1959) Conduction of heat in solids. Clarendon Press, Oxford
3. Croft DR, Lilley DG (1977) Heat transfer calculations using finite difference equations. Applied Science Publishers, Ltd, London
4. Friedmann EI (1977) Microorganisms in Antarctic desert rocks from dry valleys and Dufek Massif. Antarc J US 12:26–30
5. Friedmann EI (1982) Endolithic microorganisms in the Antarctic cold desert. Science 215: 1045–1053.
6. Friedmann EI, Galun M (1974) Desert algae, lichens, and fungi. In: Brown GW (ed) Desert biology, vol II. Academic Press, New York, pp 165–212
7. Friedmann EI, Ocampo R (1976) Endolithic blue-green algae in the dry valleys: primary producers in the Antarctic desert ecosystem. Science 193:1247–1249
8. Friedmann EI, Ocampo-Friedmann R (1984) Endolithic microorganisms in extreme dry environments: analysis of a lithobiontic microbial habitat. In: Reddy CA (ed) Current perspectives in microbial ecology. American Society for Microbiology, Washington, DC, pp 177–185
9. Friedmann EI, Ocampo-Friedmann R (1984) The Antarctic cryptoendolithic ecosystem: relevance to exobiology. Origins of Life 14:771–776
10. Friedmann EI, Weed R (1987) Microbial trace-fossil formation, biogenous, and abiotic weathering in the Antarctic cold desert. Science 236:703–705
11. Friedmann EI, McKay CP, Nienow JA (1987) The cryptoendolithic microbial environment in the Ross Desert of Antarctica: continuous nanoclimate data, 1984 to 1986. Polar Biol 7: 273–287
12. Gates DM (1980) Biophysical ecology. Springer-Verlag, New York

13. Graser AE, Van Bavel CHM (1982) The effect of soil moisture upon soil albedo. Agric Meteorol 27:17–27
14. Jaag O (1945) Untersuchungen über die Vegetation und Biologie der Algen des Nackten Gesteins in den Alpen, im Jura und im schweizerischen Mittelland. Beiträge zur Kryptogamenflora der Schweiz. Band 9, Heft 3
15. Jones HG (1983) Plants and microclimate. Cambridge University Press, New York
16. Kappen L, Friedmann EI (1983) Ecophysiology of lichens in the dry valleys of southern Victoria Land, Antarctica. II. CO_2 gas exchange in cryptoendolithic lichens. Polar Biol 1:227–232
17. Kappen L, Friedmann EI, Garty J (1981) Ecophysiology of lichens in the dry valleys of southern Victoria Land, Antarctica. I. Microclimate of the cryptoendolithic lichen habitat. Flora 171: 216–235
18. Kershaw KA (1983) The thermal operating-environment of a lichen. Lichenologist 15: 191–207
19. McCullough EC, Porter WP (1971) Computing clear day solar radiation spectra for terrestrial ecological environments. Ecology 52:1008–1015
20. McKay CP, Friedmann EI (1985) The cryptoendolithic microbial environment in the Antarctic cold desert: temperature variations in nature. Polar Biol 4:19–25
21. Miotke F-D (1979) Zur physikalischen Verwitterung im Taylor Valley, Victoria-Land, Antarktis. Polarforschung 49:117–142
22. Monteith JL (1973) Principles of environmental physics. Edward Arnold, Ltd, London
23. Müller G (1967) Methods in sedimentary petrology. Hafner Publishing Company, New York
24. Nienow JA, Meyer MA (1988) Biologically relevant physical measurements in the Ross desert: soil temperature profiles and UV radiation. Antarct J US 21(5):222–224
25. Robinson N (1966) Solar radiation. Elsevier Publishing Company, New York
26. Stearns CR (1982) Antarctic automatic weather stations. Antarc J US 17:217–219
27. Stearns CR, Savage ML (1981) Automatic weather stations. Antarc J US 16:190–192
28. Swinbank WC (1963) Longwave radiation from clear skies. Quart J Roy Meteorol Soc 89: 339–348
29. Vestal JR, Federle TW, Friedmann EI (1984) The effects of light and temperature on the Antarctic cryptoendolithic microbiota in vitro. Antarc J US 19:173–174